International Journal of Nanoelectronics and Materials
Volume 16 (Special Issue) December 2023 [143-153]

Terahertz Imaging Using Nanorectifier-Based Detectors and Broadband Thermal Sources

Shahrir R. Kasjoo[1,2,*], Arun K. Singh[3], Claudio Balocco[4] and Aimin Song[5]

[1]Faculty of Electronic Engineering & Technology, Universiti Malaysia Perlis (UniMAP), 02600 Arau, Perlis, Malaysia
[2]Institute of Nano Electronic Engineering, Universiti Malaysia Perlis (UniMAP), 01000 Kangar, Perlis, Malaysia
[3]Department of Electronics and Communication Engineering, Punjab Engineering College (Deemed to be University), Sector-12, Chandigarh-160012, India
[4]Department of Engineering, Durham University, DH1 3LE Durham, United Kingdom
[5]Department of Electrical & Electronic Engineering, University of Manchester, M13 9PL Manchester, United Kingdom

ABSTRACT

Several terahertz imaging experiments have been conducted at room temperature using a self-switching diode (SSD) rectenna as a detector, and a broadband thermal source (at 610 °C) as a continuous-wave terahertz generator. Since the terahertz emission produced by the source is non-coherent with random polarizations and has a wide-ranging spectrum, the SSD-based rectenna employed in this work utilizes a planar spiral micro- antenna which has a circular polarization that able to effectively capture all incident radiation regardless of the angles. The antenna has been designed for a broadband frequency response in the range of 0.1-10 THz. This is to ensure the terahertz images produced are ascribed to the terahertz radiation collected by the antenna, but without eliminating the possibility of thermal effects at frequencies higher than the terahertz region. In order to further validate the results obtained, an Airy pattern experiment has been conducted. Based on this experiment, the effective frequency response of the SSD rectenna is estimated at 2.29 THz. The utilization of thermal source and micro-size rectenna in this work may pave the way to explore many opportunities in developing flexible, compact, and low-cost terahertz imaging systems without the use of expensive components (e.g., typically lasers are used as terahertz sources).

Keywords: Diode, rectenna, spiral micro-antenna, terahertz imaging, thermal source

1. INTRODUCTION

Within the electromagnetic spectrum, the terahertz (THz) frequency band lies between millimeter wave and infrared (IR) regions. It encompasses electromagnetic waves spanning frequencies from 0.1 to 10 THz. The associated photon energy and wavelength are in the range of 0.4-40 meV and 3-0.03 mm, respectively [1-2].

Recently, THz-based technology has received considerable interest due to its remarkable potential across numerous applications. The most attractive property of THz waves is their ability to penetrate several dielectric materials that are opaqued to the visible light, such as textiles, plastics, and papers [2-4]. This unique feature of THz radiation allows its utilization in various commercial applications. For instance, THz imaging systems are used in non-invasive human screenings designed for public security [5], as well as in the inspection of items within containers made of plastics or cardboards to ensure the industrial quality controls are very well in place [6].

* Corresponding authors: shahrirrizal@unimap.edu.my

Nevertheless, most of the THz-related instruments have some disadvantages, such as being relatively high costs, substantial size, or restricted operation under extremely low temperature [2,4,7]. These limitations might impede the progressive advancement of THz devices. Therefore, one of the main motivations behind this work is to develop THz systems that are adaptable, compact, and economical. Here, we report on the development of a cost-effective and compact THz imaging system based on planar nanorectifier, namely the self-switching diode (SSD), as a detector, and an inexpensive blackbody source as a continuous-wave THz generator that can produce a broadband thermal radiation at THz frequencies (dependent on the setting temperature of the source) with considerable amount of power. The details of SSD including its working principle and operation at high frequencies (up to THz) can be found elsewhere [8-11].

2. BLACKBODY RADIATION

A blackbody is defined as an ideal body that is able to absorb all electromagnetic radiation with various frequencies and angles of incidence. At thermal equilibrium state, the spectrum of electromagnetic radiation emitted by a blackbody is governed by Planck's law [12],

$$B_f(T) = \frac{2hf^3}{c^2\left(\exp\left(\frac{hf}{kT}\right)-1\right)} \quad (1)$$

where B_f and T are the spectral radiance and the absolute temperature, respectively. The symbols of h, f, c and k are the Planck's constant, the frequency, the light speed, and the Boltzmann's constant, respectively. Based on Equation (1), the spectrum of a blackbody radiation at different temperatures can be plotted as shown in Figure 1 [13].

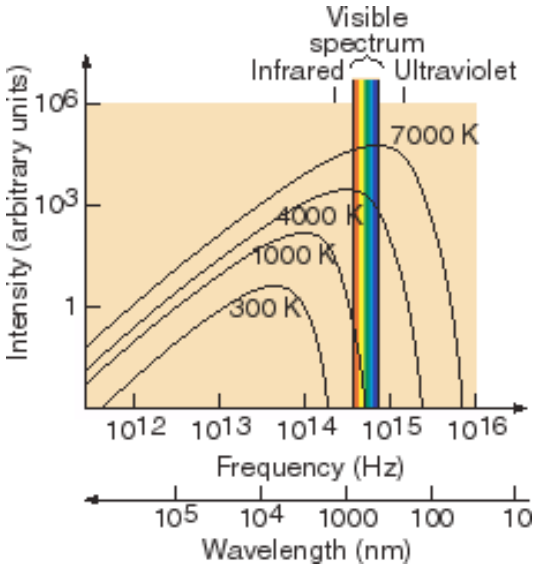

Figure 1. An electromagnetic radiation spectrum emitted by a blackbody based on Planck's law, at different temperatures. The infrared, ultraviolet and visible spectrum are also shown [13].

By referring to the Wien's displacement law, the frequency of the peak intensity of the spectrum, f_{peak} at different T can be estimated using the following equation, $f_{peak} = bT$, where b is a constant, assuming that $f \gg kT$ from Equation (1) [12].

3. EXPERIMENTAL SET UP

As mentioned earlier, an SSD-based rectenna, consisted of an SSD array coupled with a spiral antenna [see Figures 2(a) and (b)], has been utilized to detect a blackbody radiation generated by a thermal source. For device operation in the THz frequency range, a GaAs/AlGaAs quantum well wafer, grown by molecular-beam epitaxy method, has been chosen whereby the rectenna was fabricated onto this heterostructure material. The quantum well was located 50 nm below the wafer surface forming a 2-D electron gas (2-DEG) layer. Based on Hall's measurement, the electron mobility and carrier density of this material at room temperature were 7,000 cm^2/Vs and 6.0×10^{11} cm^{-2}, respectively, and at 77 K were 72,000 cm^2/Vs and 5.6×10^{11} cm^{-2}, respectively. The schematic diagram of the material used in the fabrication of the device is illustrated in Figure 2(c). The rectenna was affixed to a board which was then inserted into a holder [see Figure 2(d)]. Its current-voltage (I–V) characteristic, measured at room temperature, can be observed in Figures 3(a) and (b), which has a typical diode-like behaviour that can be utilized to rectify electrical signals.

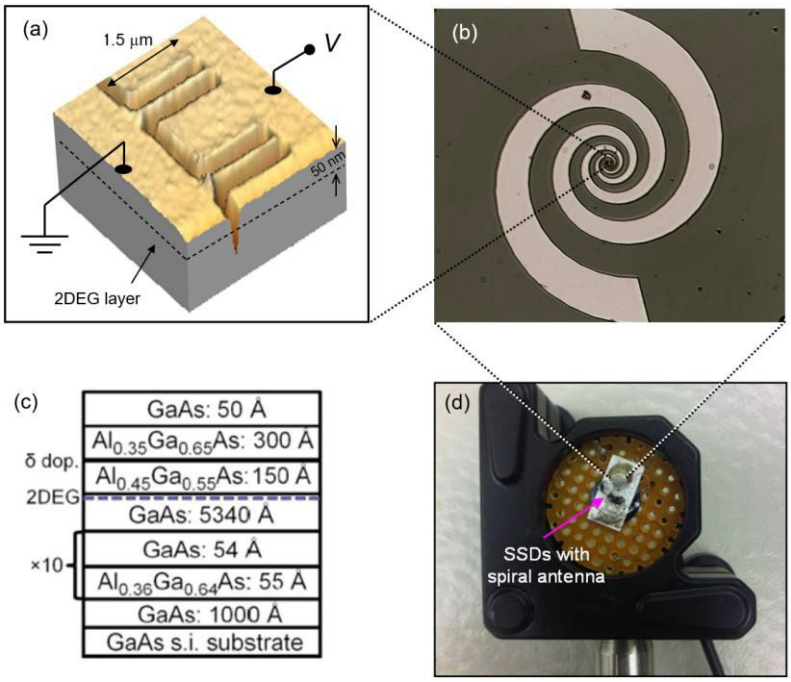

Figure 2. (a) 3-D rendering of an atomic-force microscope (AFM) image of the SSD array. (b) Optical image of the rectenna, consisting of SSD array and planar spiral antenna. (c) Schematic diagram of the GaAs/AlGaAs-based material used in the device fabrication. 2-DEG layer was formed 50 nm below the wafer surface. (d) Picture of the SSD-based rectenna, affixed to a board and fitted into a holder.

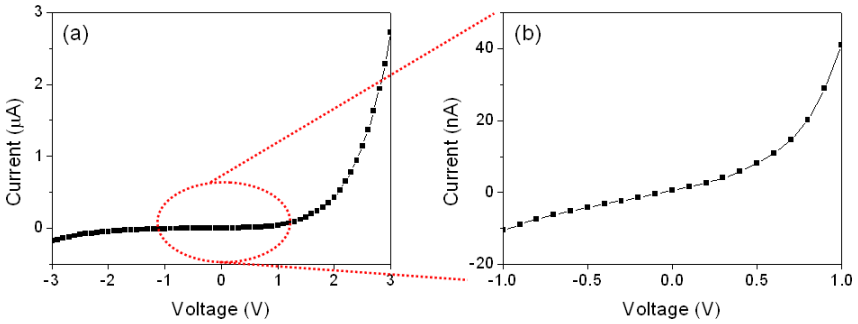

Figure 3. I-V characteristic of the rectenna with applied voltage from (a) -3 V to 3 V. (b) -1 V to 1 V.

Figure 4 shows the diagram of the experimental arrangement designed to generate THz images. Radiation from the thermal source was transmitted through an aperture and then directed towards the sample under observation. This sample was placed on a computer controlled XYZ scanning stage driven using a step motor. By means of an off-axis parabolic mirror, the radiation beam that passed through the sample was focused onto the rectenna. Prior to that, the beam was modulated at 200 Hz by an optical chopper. The rectified output voltage produced by the rectenna was then measured and computed. These were conducted using a lock-in amplifier (Signal Recovery, model 7265 DSP) with the reference frequency input provided by the chopper. The recorded data was utilized using a computer to generate an image which was produced one pixel at a time. In order to verify this imaging set up, a conventional Golay cell IR detector was employed to capture images of several millimeter-sized holes of a circuit board [see Figures 5(a) and (b)]. In this case, the temperature of the thermal source was set at 300 °C.

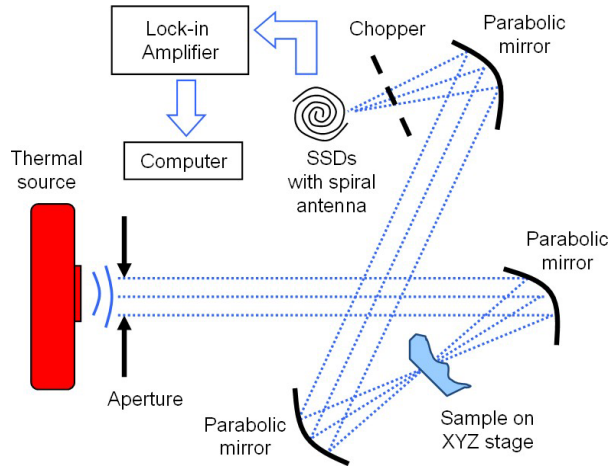

Figure 4. Illustration of the THz imaging set up. The blackbody radiation beam from the thermal source that passed through the targeted object (positioned on XYZ scanning stage) was modulated by an optical chopper and was then directed towards the SSD-based rectenna. The rectified voltage was measured and computed by a lock-in amplifier connected to a computer which generated the image one pixel at a time.

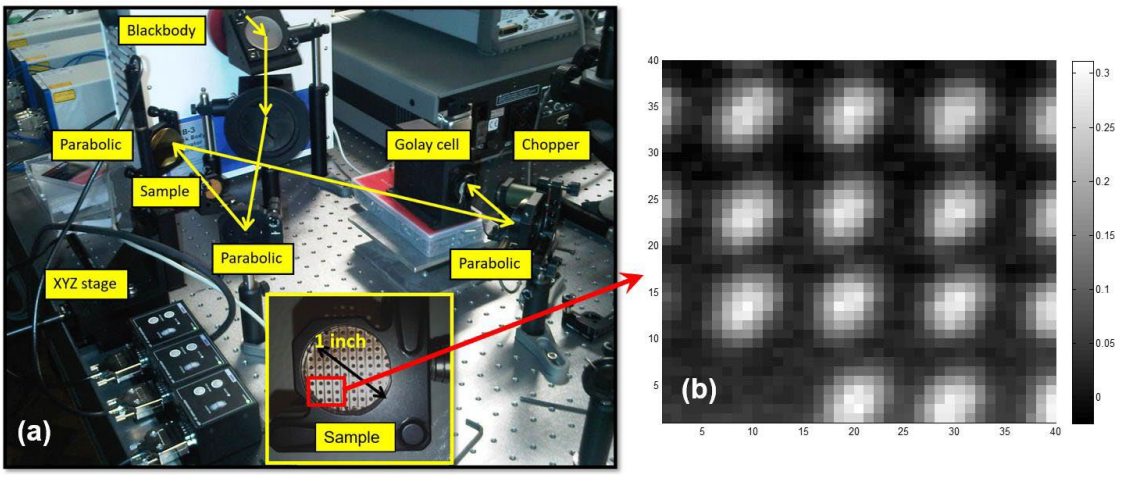

Figure 5. (a) Picture of the imaging set up. The set up was verified using a standard Golay cell as an IR detector to image several millimeter holes on a circuit board (see inset) with thermal source set at 300 °C. The inset shows the circuit board that has been fitted into a holder. (b) Final image (40 × 40 pixels) of the holes. Each pixel size is 0.25 × 0.25 mm. The white region indicates the highest rectified output voltage whereby blackbody radiation was able to pass through the holes and detected by the rectenna.

Before conducting the imaging procedure using the SSD-based rectenna, the output voltage, V_{out} of the rectenna was measured with various temperatures of the thermal source as displayed in Figure 6. The identical arrangement set up was employed but with the absence of a sample on the XYZ stage. The rectenna yielded its highest output when the thermal source was operating at its maximum temperature (i.e., 610 °C). At below 300 °C, the output levels were notably minimal, and the measured V_{out} became unstable. This behaviour is expected since at any detected frequency, decreasing the temperature will reduce the intensity of the radiation emitted by the thermal source (refer to Figure 1), and hence, lowering the amount of V_{out}.

Based on this result, the millimeter-sized holes of the circuit board were imaged again, but this time, the SSD-based rectenna was used as the detector, and the thermal source temperature was stabilized at 500 °C. The imaging process has been carried out at room temperature and in the dark. The outcomes are shown in Figures 7(a) and (b), illustrating two-dimensional and three-dimensional orientations, respectively. As can be seen, the radiation beam (generated by the thermal source) that passed through the holes can be captured and rectified by the rectenna. Since each hole was approximately 1-mm diameter in size, the spatial resolution of the rectenna can be lower than this dimension.

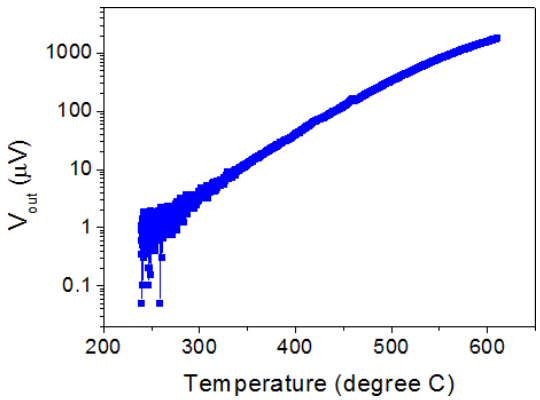

Figure 6. V_{out} with respect to the temperature of the thermal source. At below 300 °C, the measurement was unstable due to the low radiation of the thermal source.

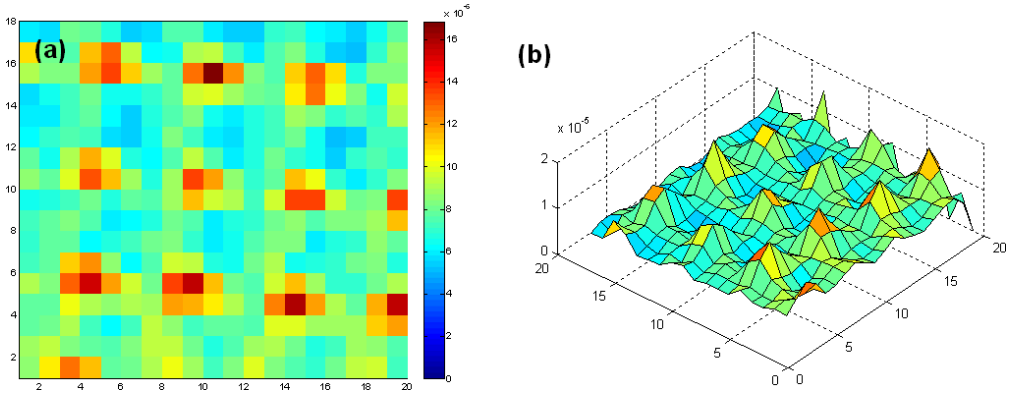

Figure 7. (a) Final image (20 ×18 pixels) of the millimeter-sized holes of the circuit board produced by means of an SSD-based rectenna with thermal source stabilized at 500 °C. Each pixel size is 0.5 x 0.5 mm. Scale on the right of the image provides reference values of V_{out} . (b) Three-dimensional orientation of the image obtained in (a).

4. RESULTS AND DISCUSSION

Since THz waves are able to penetrate plastic, in this work, several objects concealed beneath this material have been imaged using SSD-based rectenna detector. This has been conducted at room temperature and in the dark, with the thermal source stabilized at temperature of 610 °C. All resulting images were standardized to dimensions of 50 × 50 pixels. The size of each pixel was 0.4 × 0.4 mm, representing its corresponding measured value of V_{out} displayed in log scale.

In Figure 8, the image obtained from scanning a USB pen drive shows that the radiation beam was capable of penetrating the pen drive's plastic cover, but it was reflected by the USB connector made of metallic material. In the case of a marker pen, the plastic cap allowed the beam to pass through, but the liquid ink underneath the cap acted as a barrier to the radiation, as shown in Figure 9. Likewise, the presence of water in the freshly cut leaf veins has resulted in a lower transmission of the radiation beam as can be observed in Figure 10.

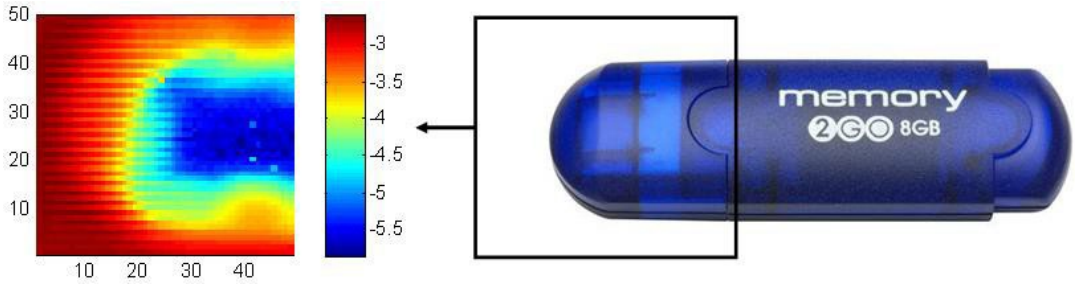

Figure 8. Scanned image of a USB pen drive. Radiation emitted by thermal source was able to pass through the plastic cover but was reflected by the USB connector made of metallic material.

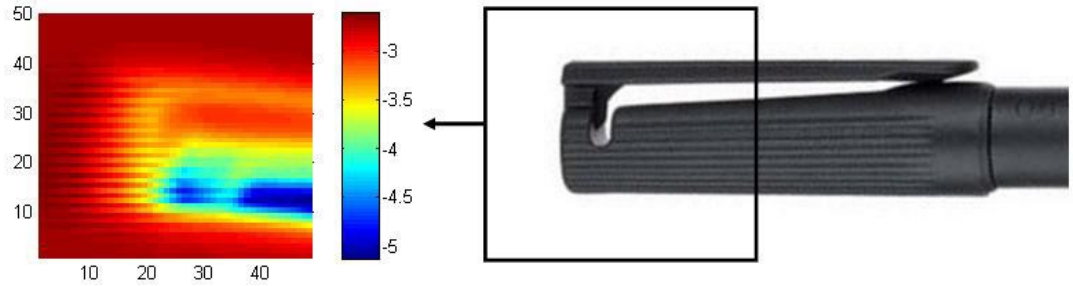

Figure 9. Scanned image of a marker pen. The plastic cap was transparent to the radiation beam from the thermal source, but the beam was blocked by the liquid ink beneath the cap.

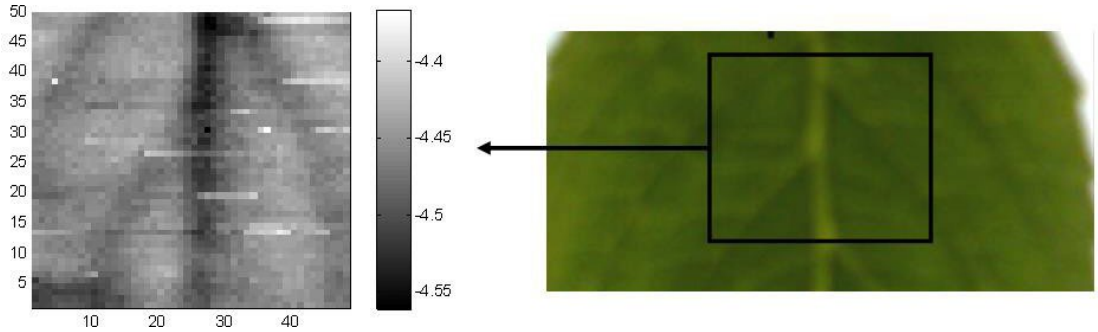

Figure 10. Scanned image of a freshly cut leaf. The existence of water in the vein structures of the leaf resulted in a lower transmission of the radiation beam from the thermal source.

Due to radiation, the thermal source set at 610 °C, was expected to exhibit $f_{peak} \sim 90$ THz. However, since the radiation spectrum was broad, the thermal source operating at this temperature also emitted radiation that is possessed in the THz region. In fact, the detector's spiral antenna was primarily designed with the effective frequency bandwidth within this THz range [14]. As mentioned earlier, the small SSD array utilized in this detector has been fabricated using a high-mobility 2-DEG heterostructure material. Based on Monte-Carlo simulations, the device was predicted to have an enhanced THz rectifying feature just before its cut-off frequency which falls within 1–3 THz [9, 15]. Therefore, the frequency response of the rectenna was expected to have an effectively narrow bandwidth, centered approximately at 2 THz. To find out this central frequency, an Airy pattern experiment was conducted (based on the theory of the diffraction of light). Further details of this experiment will be discussed later.

Nevertheless, if the actual effective frequency bandwidth of the rectenna was wide, the possibility that the objects in Figures 8-10 were imaged at frequencies beyond the THz region must also be considered (i.e., IR imaging instead of THz imaging). In the case of the freshly cut leaf, it was feasible for the IR radiation beam from the thermal source to penetrate the leaf which has a thickness of less than a millimeter. The leaf's veins have a higher thickness, and hence resulted in the lower transmission of the radiation. However, it is worth noting that IR radiation can only penetrate a few millimeters into an object [15]. Hence, when evaluating the scanned images of the USB pen drive and marker pen, the possibility of employing different IR imaging methods (commonly referred to as thermal imaging) can also be taken into account.

In thermal imaging system, the material emissivity provides the relation between the radiation power emitted by the material's surface and its temperature. A surface with a low emissivity value such as steel and aluminum, effectively behaves as a mirror (i.e., displaying high reflectance), in contrary to materials such as water and plastic, each of which possesses a surface with a high value of emissivity. For an active imaging approach, the presence of temperature differences on the surface of a particular material indicates the possibility for detecting any changes within the subsurface of that material due to the different thermal diffusivity characteristics. This explains that the IR radiation might contribute to the imaging results of the USB pen drive and marker pen.

Moreover, in thermal imaging, the commonly used spectral bands are 2–5.6 μm (i.e., 53.6– 150 THz) and 8–14 μm (i.e., 21.4–37.5 THz) due to their low atmosphere absorption [16]. These frequency bands are still within the spectrum of the radiation emitted by the thermal source that has been set to a temperature of 610 °C.

5. AIRY PATTERN EXPERIMENT

When an electromagnetic radiation beam passes through a circular aperture, it gives rise to a diffraction pattern recognized as the Airy pattern. This pattern comprises a central bright area, referred to as the Airy disc, surrounded by a sequence of concentric bright rings as shown in Figures 11(a) and (b). Both Airy pattern and Airy disc are attributed to George Biddell Airy, who authored the comprehensive theoretical explanation on the appearance of disc and rings phenomenon when observing a bright star through a high magnification telescope [17].

According to Fraunhofer diffraction theory, an Airy pattern can only be observed at a distance, $R > D^2/\lambda$. This distance is far from an aperture. Here, R represents the distance from the center-axis of the aperture with diameter D, at which the first minimum intensity of the Airy pattern becomes evident, and λ is the beam's wavelength (see Figure 12). The incoming beam towards the aperture must be a plane wave with uniform intensity across the aperture's entire area. This can be achieved by positioning the radiation source far from the aperture.

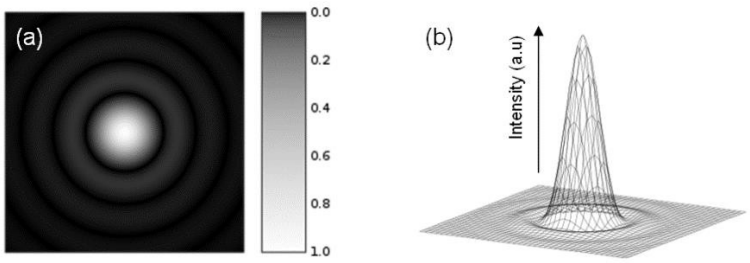

Figure 11. Example of an Airy pattern image which has a central bright area known as Airy disc, and sequences of concentric bright rings surrounding the disc. The right scale of the image indicates the intensity of the pattern. (b) Example of surface plot of intensity for an Airy pattern. (Source: Wikipedia)

Figure 12. Illustration of the experimental set up for the Airy pattern imaging. Thermal source was stabilized at 610 °C to generate radiation and pass through an optical chopper and a small aperture with a diameter of 1.5 mm. To detect a possible airy pattern image, a raster scanning was conducted by utilizing a rectenna placed on XYZ stage with L = 5.6 cm. The desired output was read out by means of a lock-in amplifier, and the final image was generated using a computer. The value of X can then be estimated, which can be used to figure out the rectenna's effective frequency response.

Figure 12 shows the illustration arrangement of the experimental set up. A thermal source was set at temperature of 610 °C to produce a similar transmitted beam as in the earlier imaging experiment. The thermal source was placed at more than 15 cm away from an aperture with a diameter of 1.5 mm. An optical chopper was used to modulate the beam. To determine the SSD-based rectenna's effective frequency response, f_{eff}, the rectenna was employed to image a possible Airy pattern through the utilization of an XYZ scanning-stage. The rectenna was positioned at L = 5.6 cm away from centre-axis of the aperture. Assuming the angle between L and R (i.e., θ) was extremely small, then $R \sim L$. From previous section, the value of f_{eff} was predicted around 2 THz. Hence, the value of R will be bigger than $D2/\lambda$. This value obeyed the Fraunhofer diffraction theory, as mentioned earlier.

A lock-in amplifier with the reference input frequency provided by a chopper was utilized to measure the rectified output voltage of the rectenna, V_{out} which was used to generate the desired image one pixel at a time (see Figure 13) using a computer. The final image has 50 × 50 pixels, and the size of each pixel was 0.4 × 0.4 mm. The image can be used to estimate the radius of the first ring in the Airy pattern, X which was found to be approximately 6 mm.

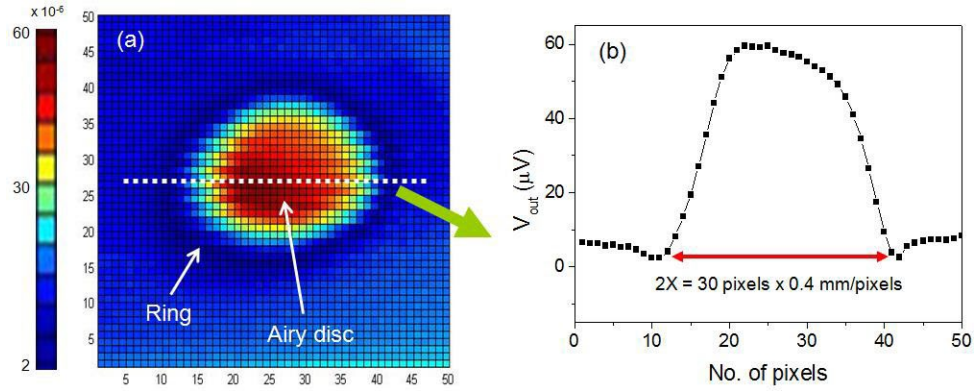

Figure 13. (a) Airy pattern image generated by utilizing an SSD-based rectenna. The image has 50 x 50 pixels, and the size of each pixel was 0.4 x 0.4 mm. Airy disc is the area where V_{out} has a high value, which can be mainly observed in the center of the pattern image. The minimum value of V_{out} , indicated by the dark blue region, formed a ring around the disc. (b) The plot of V_{out} with respect to the image pixels, based on the dotted line cross-section in (a). From the graph, the estimated value of X was 6 mm.

According to the Fraunhofer diffraction theory, the Airy pattern intensity can be written as [18],

$$I(\theta) = I_0 \left[\frac{2J_1(x)}{x}\right]^2 \quad (2)$$

where I_0 is the maximum intensity at the center of the Airy disc, J_1 is the Bessel function of the first kind of order first, and $x = KD \sin(\theta)$ in which $K = 2\pi/\lambda$. The zeros of J_1 can be estimated when x = KD sin $(\theta) \approx 0$, 3.8317, 7.0156, 10.1735 and so on. Therefore, the first ring in the Airy pattern occurs at x = KD sin $(\theta) \approx 3.8317$, which can be reworked as [18],

$$\sin(\theta) = \frac{1.22\lambda}{D} \tag{3}$$

Substituting sin $(\theta) = X/R$ and $f_{eff} = c/\lambda$ into Equation (3) would yield $f_{eff} \sim 2.29$ THz, which almost agreed with the predicted value.

6. CONCLUSION

This work has successfully presented the initial implementation of active THz imaging using an SSD-based rectenna at room temperature, albeit with an experimental set up that has not been fully optimized. The obtained results are not only supported by the previous simulation studies on THz spiral antenna [14] and THz rectification by SSDs [8-11], but also verified by the Airy pattern experiment demonstrated in this work. Although it is possible that the generated images could also be influenced by thermal effects in frequency ranges higher than the THz region, nevertheless the SSD-based rectenna has displayed its practical application as a detector within the active imaging system.

Moreover, owing to the planar nature of the SSD structure, it becomes feasible to fabricate a matrix with numerous SSDs connected to antennas via a cost-effective nanoimprinting lithography technique, all in a single-step process [19]. Consequently, a multi-pixel THz detector can be realized whereby each rectenna cell serves as a single-pixel unit. With further optimization of the rectenna's detection properties, including achieving low noise-equivalent power [20, 21] and implementing advanced antenna designs [22, 23], the SSD-based technology possesses a significant potential for future THz electronic nanodevices. Furthermore, this work might be useful to other types of planar device technologies such as, geometric diodes [24], planar barrier diodes [25], ballistic rectifiers [26], and metal-insulator-metal (MIM) diodes [27].

ACKNOWLEDGEMENTS

The authors would like to acknowledge to all those who have provided assistance and made valuable contributions to the achievement of this work.

REFERENCES

[1] Sizov, F. F., Semiconductor Physics, Quantum Electronics & Optoelectronics vol 22, issue 1 (2019) pp. 67-79.
[2] Kasjoo, S. R., Mohd Mokhar, M. B., Zakaria, N. F., Juhari, N. J., AIP Conference Proceedings vol 2203 (2020) pp. 020020-1-020020-8.
[3] Huang, Yi., Shen, Y., Wang, J., Engineering vol 22 (2023) pp. 106-124.
[4] Valusis, G., Lisauskas, A., Yuan, H., Knap, W., Roskos, H. G., Sensors vol 21, issue 12 (2021) pp. 4092-1-4092-51.
[5] Li, L., Xue, F., Liang, D., Chen, X., Appl. Sci. vol 11, issue 23 (2021) pp. 11241-1-11241-16.
[6] Mao, Q., Liu, J., Zhu, Y., Lv, C., Lu, Y., Wei, D., Yan, S., Ding, S., Ling, D., IEEE Transaction on Terahertz Science and Technology vol 11, issue 5 (2021) pp. 583-590.
[7] Bai, P., Zhang, Y., Wang, T., Fu, Z., Shao, D., Li, Z., Wan, W., Li, H., Cao, J., Guo, X., Shen, W., Nature Communications vol 10 (2019) pp. 3513-1-3513-9.

[8] Song, A. M., Missous, M., Omling, P., Peaker, A. R., Samuelson, L., Seifert, W., Applied Physics Letters vol 83, issue 9 (2003) pp. 1881-1883.
[9] Mateos, J., Vasallo, B. G., Pardo, D., Gonzalez, T., Appl. Phys. Lett. vol 86, issue 21 (2005) pp. 212103-1-212103-3.
[10] Balocco, C., Kasjoo, S. R., Lu, X. F., Zhang, L. Q., Alimi, Y., Winnerl, S., Song, A. M., Appl. Phys. Lett. vol 98, issue 22 (2011) pp. 223501-1-223501-3.
[11] Kasjoo, S. R., Singh, A. K., Mat Isa, S. S., Ramli, M. M., Mohamad Isa, M., Ahmad, N., Mohd Nor, N. I., Khalid, N., Song, A. M., Solid-State Electronics vol 118 (2016) pp. 36-40.
[12] Schlessinger, M., "Infrared Technology Fundamentals," 2nd ed., rev. and expanded, Marcel Dekker Inc., (1995) pp. 1-462.
[13] Chaisson, E., McMillan, S., "Astronomy Today," 9th ed., Pearson, (2017) pp. 59-77.
[14] Choudhry, S. H., "Antenna Design for Terahertz Nanodevices," M. Phil. Thesis, The University of Manchester (2009).
[15] Xu, K. Y., Lu, X. F., Song, A. M., Wang, G., J. Appl. Phys. vol 103, issue 11 (2008) pp. 113708-1-113708-8.
[16] Avdelidis, N. P., Moropoulou, A., Almond, D. P., Proc. SPIE vol 5612 (2004) pp. 126-140.
[17] Airy, G. B., Transactions of the Cambridge Philosophical Society vol 5 (1835) pp. 283-291.
[18] Serway, R. A., Jewett Jr, J. W., "Physics for Scientists and Engineers with Modern Physics," 7th ed., Thomson Learning Inc., (2008) pp. 1077-1110.
[19] Lausecker, E., Huang, Y., Fromherz, T., Sturm, J. C., Wagner, S., Appl. Phys. Lett. vol 96, issue 26 (2010) pp. 263501-1-263501-3.
[20] Balocco, C., Kasjoo, S. R., Zhang, L. Q., Alimi, Y., Song, A. M., Appl. Phys. Lett. vol 99, issue 11 (2011) pp. 113511-1-113511-3.
[21] Kasjoo, S. R., Singh, A. K., Balocco, C., Song, A., International Journal of Nanoelectronics and Materials vol 14, special issue (2021) pp. 53-58.
[22] Etor, D., Dodd, L. E., Wood, D., Balocco, C., "Impedance matching at terahertz frequencies: Optimizing power transfer in rectennas," in Proc. 40th International Conference on Infrared, Millimeter, and Terahertz Waves (IRMMW-THz), Hong Kong, (2015), 15599188.
[23] Mohd Mokhar, M. B., Kasjoo, S. R., Juhari, N. J., "Simulation of terahertz broadband antennas for rectenna applications," in Proc. 32nd International Conference on Microelectronics (ICM), Aqaba, Jordan, (2020), 20386807.
[24] Zhu, Z., Joshi, S., Moddel, G., IEEE Journal of Selected Topics in Quantum Electronics vol 20, issue 6 (2014), pp. 3801409.
[25] Zakaria, N. F., Kasjoo, S. R., Zailan, Z., Mohamad Isa, M., Md Arshad, M. K., Taking, S., Jpn. J. Appl. Phys. vol 57, issue 6 (2018), pp. 064101-1-064101-7.
[26] Singh, A. K., Kasjoo, S. R., Song, A. M., IEEE Transactions on Nanotechnology vol 13, issue 3 (2014), pp. 527-531.
[27] Etor, D., Dodd, L. E., Wood, D., Balocco, C., Appl. Phys. Lett. Vol 109, issue 19 (2016), pp. 193110-1-193110-4.